Compact diode-pumped continuous wave and passively Q switched Tm:YAG laser at 2.33 μm

Fangyuan Zha, Xiaoxu Yu, Hongwei Chu, Han Pan, Shengzhi Zhao, Pavel Loiko, Zhongben Pan, Dechun Li

Compact diode-pumped continuous-wave and passively Q-switched Tm:YAG laser at 2.33 μm

Fangyuan Zha,[1] Xiaoxu Yu,[1] Hongwei Chu,[1] Han Pan,[1] Shengzhi Zhao,[1] Pavel Loiko,[2] Zhongben Pan[1,2] and Dechun Li[1,3]

[1] *School of Information Science and Engineering, Shandong University, Qingdao 266237, China*
[2] *Centre de Recherche sur les Ions, les Matériaux et la Photonique (CIMAP), UMR 6252 CEA-CNRS-ENSICAEN, Université de Caen Normandie, 6 Boulevard Maréchal Juin, 14050 Caen Cedex 4, France*
[2]*e-mail: zhongbenpan@sdu.edu.cn*
[3]*e-mail: dechun@sdu.edu.cn*

Received XX Month XXXX; revised XX Month, XXXX; accepted XX Month XXXX; posted XX Month XXXX (Doc. ID XXXXX); published XX Month XXXX

Compact diode-pumped continuous-wave (CW) and passively Q-switched Tm:YAG lasers operating on the $^3H_4 \rightarrow {}^3H_5$ transition are demonstrated. Using a 3.5at. % Tm:YAG crystal, a maximum CW output power of 1.49 W was achieved at 2330 nm with a slope efficiency of 10.1%. The first Q-switched operation of the mid-infrared Tm:YAG laser was realized with a few-atomic-layer MoS_2 saturable absorber. Pulses as short as 150 ns were generated at a repetition rate of 190 kHz, corresponding to a pulse energy of 1.07 μJ. Tm:YAG is an attractive material for diode-pumped CW and pulsed mid-infrared lasers emitting around 2.3 μm. © 2022 Optica Publishing Group

Yttrium aluminum garnet ($Y_3Al_5O_{12}$, YAG) is one of the most widely used laser host crystals for doping with rare-earth ions (RE^{3+}). It offers good thermo-mechanical properties making it possible the development of high-power laser systems. The RE^{3+} ions in YAG exhibit relatively large Stark splitting of their multiplets (owing to a strong crystal-field), as well as long emission lifetimes. Moreover, RE^{3+}-doped YAG can be easily grown by the Czochralski method.

YAG has been employed as a host matrix for thulium (Tm^{3+}) ions (electronic configuration: $[Xe]4f^{12}$) for achieving laser emission at ~2 μm according to the $^3F_4 \rightarrow {}^3H_6$ electronic transition [1]. Tm^{3+} shows strong absorption at ~0.8 μm (the $^3H_6 \rightarrow {}^3H_4$ transition) and can be efficiently pumped by commercial AlGaAs laser diodes. Tm^{3+} ions in YAG exhibit a relatively large splitting of the ground-state ($^3H_6$), 768 cm^{-1} [2], so that their emission extends beyond 2 μm which is attractive for broadly tunable [3] and mode-locked lasers [4]. Efficient and high-power Tm:YAG lasers emitting at 2 μm have been demonstrated, including thin-disk ones [1,5,6].

Other transitions of Tm^{3+} ions are also noteworthy, originating from the $^3H_4$ state, corresponding to emission at ~1.5 μm ($^3H_4 \rightarrow {}^3F_4$) and ~2.3 μm ($^3H_4 \rightarrow {}^3H_5$) [7,8]. The latter one falling into the mid-infrared spectral range is of particular interest since it spectrally overlaps with multiple atmospheric and biomolecule absorption lines, such as CO, N_2O, CH_4, H_2CO and $C_6H_{12}O_6$, providing a valuable non-invasive glucose ($C_6H_{12}O_6$) blood measurement technique [9] and being practical for gas sensing [10,11]. The $^3H_4$ Tm^{3+} manifold can be subject to multiphonon non-radiative relaxation, especially for crystals with high phonon energies like YAG ($h\nu_{ph}$ = 857 cm^{-1}, compare with $h\nu_{ph}$=446 cm^{-1} for $LiYF_4$, a commonly used material for mid-infrared Tm lasers [12]). Still, Tm:YAG is a promising material for developing power-scalable 2.3 μm lasers owing to its good thermal properties facilitating diode-pumping, and broad $^3H_4 \rightarrow {}^3H_5$ emission band, as shown in Fig. 1. Indeed, it is spanning from 2.1 to 2.75 μm and the peak stimulated-emission cross-section σ_{SE} is 0.35×10^{-20} cm^2 at 2325 nm [13].

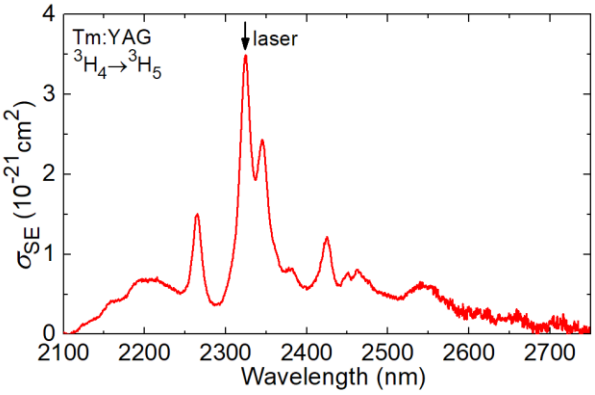

Fig. 1. Stimulated-emission (SE), cross-sections, σ_{SE}, for the $^3H_4 \rightarrow {}^3H_5$ transition of Tm^{3+} ions in YAG, *arrow* indicates the laser wavelength.

Up to date, mainly high-brightness pump sources (Ti:sapphire lasers) were applied to demonstrate mid-infrared Tm:YAG lasers. It was shown theoretically [12] and confirmed in experiment [14,15] that the slope efficiency of Tm lasers operating on the $^3H_4 \rightarrow {}^3H_5$ transition can exceed the Stokes limit owing to the positive action of the energy-transfer upconversion (ETU) from the metastable level, $^3F_4 + {}^3F_4 \rightarrow {}^3H_6 + {}^3H_4$, refilling the upper laser level. Indeed, a high

slope efficiency of 46.3% was reported in a Ti:sapphire laser-pumped Tm:YAG laser delivering 1.07 W at 2.19 and 2.33 μm [13], but its power scaling was limited. As for diode-pumping, only quasi-CW operation was demonstrated with a peak power of 1.11 W at ~2.19 and 2.32 μm corresponding to a slope efficiency of 9.1% [16]. Consequently, there is still a room for improvement of mid-infrared Tm:YAG lasers, i.e., their power scaling in the CW regime and suppressing the unwanted laser line at 2.19 μm attributed to multiphonon-assisted (vibronic) emission.

In the present work, we aimed to develop compact watt-level mid-infrared Tm:YAG lasers, as well as demonstrate for the first time their passively Q-switched operation.

The scheme of the mid-infrared Tm:YAG laser is shown in Fig. 2. Two rectangular Tm:YAG crystals with different Tm^{3+} doping levels of 2.0 and 3.5 at.% were tested. Such intermediate concentrations were selected to ensure simultaneously sufficient pump absorption and moderate cross-relaxation (CR) for Tm^{3+} ions ($^3H_6 + {}^3H_4 \rightarrow {}^3F_4 + {}^3F_4$), thus preventing the excessive quenching of the upper laser level ($^3H_4$) lifetime. The laser elements were cut along the [111] axis having an aperture of 3×3 mm^2 and a thickness of 10 and 12 mm, respectively. The crystals were polished from both sides and left uncoated. They were wrapped into a 100 μm-thick indium foil and mounted in a copper heat sink kept at 12 °C to promote the heat removal. For CW operation, a compact plane-parallel laser cavity with a geometrical length of 15 mm was used. It was formed by a flat pump mirror (PM) coated for high transmission (HT, T = 94.4%) at 0.79 μm and high reflection (HR) at 2.1-2.4 μm, and a set of flat output couplers (OCs) providing a transmission T_{OC} of 0.5% or 1% at 2.1-2.4 μm.

The pump source was a fiber-coupled AlGaAs laser diode (fiber core diameter: 200 μm, numerical aperture, N.A.: 0.22) emitting unpolarized radiation at 788-796 nm, depending on the driving current. The pump beam was refocused into the laser crystal via a 1:1 imaging module resulting in a waist radius of 100 μm. A long-pass filter was placed behind the OC to block the residual pump.

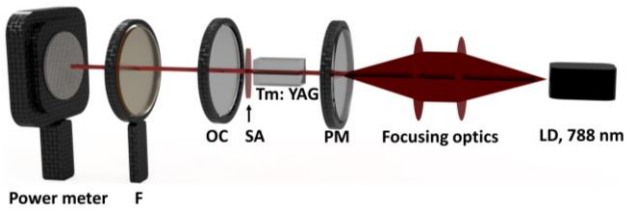

Fig. 2. Scheme of the mid-infrared Tm:YAG laser. LD: laser diode, PM: flat pump mirror, OC: flat output coupler, F: filter, SA: saturable absorber.

Few-atomic-layer molybdenum disulfide (MoS_2) is a known saturable absorber (SA) for solid-state lasers featuring broadband linear and nonlinear absorption properties, large modulation depth and ultrafast recovery time [17,18]. In the present work, a uniform large-scale MoS_2 thin film was grown on an (001) oriented single-crystal sapphire substrate (Φ 50.8 mm) by the physical vapor deposition [19]. Sapphire was selected owing to its good thermal properties facilitating heat dissipation from the SA. The as-grown MoS_2 film possessed a modulation depth of 17% with a saturation intensity I_{sat} of 1.19 MW/cm^2, and a high effective nonlinear absorption coefficient β_{eff} of −16.5 cm/MW indicating good nonlinear optical properties.

For the passively Q-switched operation, we have used a short plane-parallel cavity but with a slightly increased length of 25 mm. The 3.5 at.% Tm:YAG crystal was placed close to the PM with a small separation of ~1 mm. The distance between the output facet of the crystal and the OC was set to be ~5 mm to allow the insertion of the saturable absorber placed at normal incidence. The output coupler with a transmission of 1% was selected according to the results of the CW laser experiments.

Figure 3(a) shows the absorption cross-section spectrum of the Tm:YAG crystal around 0.8 μm (the $^3H_6 \rightarrow {}^3H_4$ Tm^{3+} transition). The peak σ_{abs} is 0.65×10^{-20} cm^2 at 786 nm and the absorption bandwidth (FWHM) is ~3 nm. Even though both studied OCs provided high reflectivity at the pump wavelength, the back reflected pump was focused behind the crystal thus almost not contributing to the gain. Thus, the absorbed pump power P_{abs} was calculated for single-pass pumping. First, the pump absorption efficiency under non-lasing (NL) conditions, $\eta_{abs,NL}$, was determined from pump-transmission measurements, Fig. 2(b). Then, the pump absorption under lasing (L) conditions was estimated from the $\eta_{abs,NL}$ value at the threshold pump power P_{th} separately for each OC (considering clamping of the level of inversion at the laser threshold). For 3.5 at.% Tm:YAG, this yielded $\eta_{abs,L}$ = 79.7% (1% OC) and 89.5% (0.5% OC).

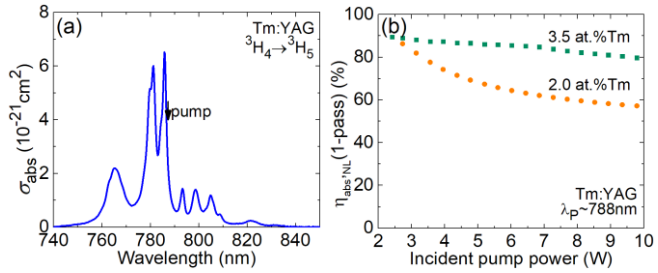

Fig. 3. Absorption of the Tm:YAG crystal: (a) absorption cross-sections, σ_{abs}, for the $^3H_6 \rightarrow {}^3H_4$ Tm^{3+} transition; (b) measured single-pass pump absorption under non-lasing (NL) conditions.

At first, we tested the 2.0 at.% Tm:YAG crystal, Fig. 4(a). For the smaller 0.5% OC, the maximum output power amounted to 0.98 W at 2.33 μm with a slope efficiency η of 9.1% (vs. the absorbed pump power). The laser threshold was at P_{th} = 2.43 W and the optical-to-optical efficiency η_{opt} was 4% (vs. the pump power incident on the crystal). For higher output coupling of 1%, the laser performance deteriorated resulting in a lower output power (0.82 W at 2.33 μm), lower slope efficiency (η = 7.6%) and increased laser threshold (P_{th} = 2.59 W).

Then, the second crystal, 3.5 at.% Tm:YAG, was inserted into the same cavity, leading to an output power of 1.03 W at 2.33 μm with a slope efficiency η of 8.7% and a laser threshold of 2.72 W (for T_{oc} = 0.5%), Fig. 4(b). For this crystal, with increasing the output coupling (T_{oc} = 1%), the output power was scaled up to 1.49 W with a higher η = 10.1% at the expense of an increased laser threshold of 3.80 W, so that the optical-to-optical efficiency η_{opt} reached 6%.

The input-output dependences were linear showing no thermal roll-over up to at least 20 W of absorbed pump power (note that a passively-cooled crystal was implemented).

The doping concentration plays a significant role for optimizing the output performance of mid-infrared Tm lasers operating on the

$^3H_4 \rightarrow {}^3H_5$ transition. Indeed, higher Tm^{3+} doping levels cause (i) stronger quenching of the upper laser level ($^3H_4$) lifetime owing to the CR process, leading to higher laser thresholds but at the same time (ii) higher pump absorption and (iii) stronger ETU refilling the $^3H_4$ manifold thus leading to higher pump quantum efficiency and potentially higher laser slope efficiency. In our case, slightly higher output power and slope efficiency were achieved for the 3.5 at.% Tm^{3+}-doped YAG crystal in agreement with the above-mentioned considerations.

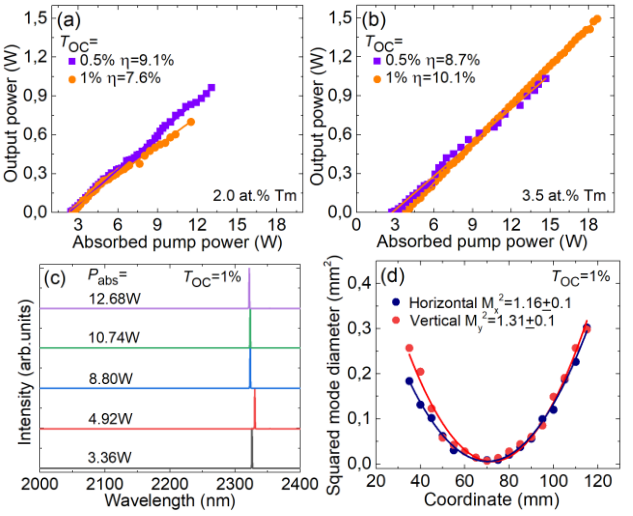

Fig. 4. CW diode-pumped mid-infrared Tm:YAG lasers: (a,b) input-output dependences, η – slope efficiency, Tm^{3+} doping level: (a) 2.0 at.%, (b) 3.5 at.%; (c) emission spectra as a function of the pump level and (d) evaluation of the beam quality factors, 3.5 at.% Tm:YAG, T_{OC} = 1%.

Table 1. Continuous-Wave Tm:YAG Lasers Operating on the $^3H_4 \rightarrow {}^3H_5$ Transition Reported So Far[a]

[b]	λ_P, nm	λ_L, μm	P_{th}, W	P_{out}, W	η, %	C_{Tm}, at.%	Ref.
TS	780	2.19, 2.33	0.86	1.07	46.3	3.2	[13]
LD	787	2.19, 2.33	1.67	1.11[c]	9.1	3.2	[16]
LD	788	2.33	2.43	0.98	9.1	2	[d]
LD	788	2.33	2.72	1.49	10.1	3.5	[d]

[a]λ_P, pump wavelength; λ_L, laser wavelength, P_{th} – laser threshold, P_{out} – maximum output power, η – slope efficiency; [b]Pump: TS, Ti:Sapphire lasers; LD, laser diodes; [c]quasi-continuous-wave operation; [d]This work.

The spectra of laser emission were weakly dependent on the output coupling and the pump power, with the main laser line located around 2.33 μm. Figure 4(c) illustrates this behavior for a fixed T_{OC} of 1% and a varied absorbed pump power. The laser linewidth (FWHM) was ~1 nm. No colasing on the competitive $^3F_4 \rightarrow {}^3H_6$ Tm^{3+} transition was observed.

The evaluation of the beam propagation factors for the mid-infrared laser based on the 3.5 at. % Tm:YAG crystal is shown in Fig. 4(d). The measured M_x^2 and M_y^2 factors are 1.16 and 1.31±0.1, respectively, indicating that the laser operated at the fundamental transverse mode. The previous reports on Tm:YAG lasers operating on the $^3H_4 \rightarrow {}^3H_5$ transition are summarized in Table 1. Compared with the previous studies, we report on both higher output power and slope efficiency for this type of lasers.

When the MoS_2-based SA was inserted into the laser resonator, stable passive Q-switching with a long-term stability was realized by slightly aligning the output coupler. This regime of operation was clearly distinct from unstable relaxation oscillations occurring in CW Tm lasers. The threshold of the laser increased to 7.3 W, while stable Q-switched operation started slightly above the threshold, at P_{abs} = 7.5 W. Under the highest absorbed pump power of 9.52 W, the maximum average output power of the passive Q-switched laser reached 204 mW at 2.33 μm (laser linewidth: 1 nm), corresponding to a slope efficiency of 9.6%, Fig. 5(a). No damage to the MoS_2-based SA was observed for the studied pump levels.

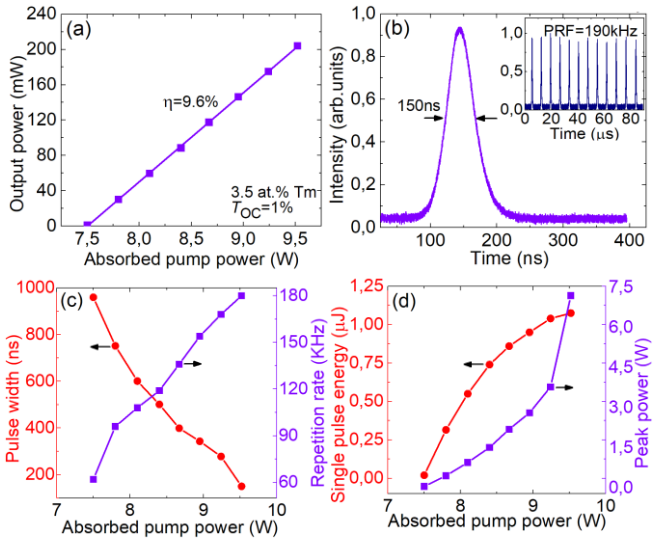

Fig. 5. Diode-pumped mid-infrared Tm:YAG laser passively Q-switched by a MoS_2-based saturable absorber: (a) input-output dependence, η – slope efficiency; (b) Oscilloscope traces of a single Q-switched pulse and a stable pulse train (*inset*); (c) pulse width and repetition rate and (d) single pulse energy and peak power all plotted versus P_{abs}.

The temporal profile of a single Q-switched pulse and that of a stable pulse train corresponding to a pulse duration (FWHM) of 150 ns and a repetition rate of 190 kHz, respectively, are given in Fig. 5(b). From the recorded pulse train, the peak-to-peak intensity instabilities were estimated to be <10%. As depicted in Fig. 5(c), the pulse duration decreased monotonically with pump power from 960 to 150 ns, while the repetition rate accordingly increased from 62 to 190 kHz. The corresponding highest single-pulse energy and the peak power amounted to 1.07 μJ and 7.15 W, respectively, at an absorbed pump power of 9.52 W, Fig. 5(d). The observed dependence of the pulse duration / energy on the pump power is typical for 2D saturable absorbers such as graphene or MoS_2 [18,20] (classified as "fast" ones for passively Q-switched lasers, i.e., showing a characteristic recovery time being much faster than that of formation of a single Q-switched pulse). It is related to the dynamic bleaching of the SA with increasing the pump power [21].

In Table 2, we present an overview of output characteristics of passively Q-switched 2.3 μm Tm lasers operating on the $^3H_4 \rightarrow {}^3H_5$ transition reported so far. We report on the shortest pulse duration ever extracted from such a laser owing to (i) the short cavity roundtrip time associated with the implemented compact laser

design and (ii) large modulation depth of the MoS_2-based SA. Note that the pulse energies for this type of lasers are usually about a few μJ due to the relatively short luminescence lifetime of the upper laser level ($^3H_4$). Indeed, for 2.0 at.% and 3.5 at.% Tm^{3+}-doped YAG, it amounts to 186 μs and 74 μs, respectively.

Table 2. Summary of Passively Q-switched Thulium Lasers at 2.3 μm Reported So Far

Crystal	SA	[a], μs	[b], KHz	[c], μJ	[d], mW	Ref.
Tm:YLF	Cr^{2+}:ZnSe	1.30	59.2	6.1	89	[22]
	Gold nanorods	0.84	6.67	[e]	320	[23]
	$ReSe_2$	0.72	5	[e]	486	[24]
	Cr^{2+}:ZnSe	1.2	2.1	13	27.3	[25]
Tm:YAP	ZIF-8@ZIF-67	0.21	128	2.74	351	[26]
	ZIF-67	0.22	95	2.31	220	[27]
	MoS_2	0.32	228	1.74	398	[19]
Tm:YAG	MoS_2	**0.15**	190	1.07	204	[f]

[a]Pulse width; [b]Repetition rate; [c]Single pulse energy; [d]Average output power; [e]Bunches of pulses; [f]This work.

To conclude, using diode-pumping and a compact laser cavity design, watt-level output at 2.33 μm is extracted from a passively-cooled Tm:YAG laser in the continuous-wave regime corresponding to a reasonably high slope efficiency of 10.1%. The latter was slightly boosted by using a 3.5 at.% Tm^{3+}-doped crystal. Still, there is a need of further optimization of the doping level to improve the pump absorption efficiency and to enhance the positive role of ETU refilling the upper laser level. The use of shorter laser crystals in this case may help to optimize the mode-matching in the cavity. Considering the excellent thermo-mechanical properties of Tm:YAG and the application of active cooling, multi-watt laser emission is expected in this way.

We also report on the first Q-switched operation of Tm:YAG at 2.33 μm. For this, a few-layer MoS_2 saturable absorber was used. To reduce the pulse duration, we have used a compact cavity design benefiting from the short roundtrip time. Pulses as short as 150 ns were generated with a repetition rate of 190 kHz, corresponding to a pulse energy of 1.07 μJ. MoS_2-based saturable absorbers thus appear as a possible alternative to Cr^{2+}:ZnSe ones. Indeed, the laser wavelength of 2.3 μm corresponds to the long-wavelength wing of the Cr^{2+} absorption band in ZnSe, so that it is difficult to provide a reasonable modulation depth at this wavelength for thin / low-doped crystals. In contrast, few-atomic-layer MoS_2 benefits from its nearly wavelength-independent linear and nonlinear absorption from the visible to mid-infrared.

Funding. National Natural Science Foundation of China (52072351, 12004213, 12174223, 21872084, 62175128). "RELANCE" Chair of Excellence project funded by the Normandy Region.

Acknowledgments. Z. Pan and H. Chu thank the financial support from Shandong University.

Disclosures. The authors declare no conflicts of interest.

Data availability. Data underlying the results presented in this paper are not publicly available at this time but may be obtained from the authors upon reasonable request.

References

1. E. C. Honea, R. J. Beach, S. B. Sutton, J. A. Speth, S. C. Mitchell, J. A. Skidmore, M. A. Emanuel, and S. A. Payne, IEEE J. Quantum Electron. **33**, 1592 (1997).
2. J. B. Gruber, M. E. Hills, R. M. Macfarlane, C. A. Morrison, G. A. Turner, G. J. Quarles, G. J. Kintz and L. Esterowitz, Phys. Rev. B. **40**, 9464 (1989).
3. R. C. Stoneman, and L. Esterowitz, Opt. Lett. **15**, 486 (1990).
4. L. J. Li, L. Zhou, T. X. Li, X. N. Yang, W. Q. Xie, X. M. Duan, Y. J. Shen, Y. Q. Yang, W. L. Yang, H. Zhang, Opt. Laser Technol. **124**, 105986 (2020).
5. J. I. Mackenzie, S.C. Mitchell, R.J. Beach, H.E. Meissner, D.P. Shepherd, Electron. Lett. **37**, 898 (2001).
6. J. Zhang, F. Schulze, K.F. Mak, V. Pervak, D. Bauer, D. Sutter, O. Pronin, Laser Photon. Rev. **12**, 1700273-1-6 (2018).
7. A. Braud, S. Girard, J.L. Doualan, M. Thuau, R. Moncorge, A.M. Tkachuk, Phys. Rev. B. **61**, 5280 (2000).
8. J. Caird, L. DeShazer, and J. Nella, IEEE J. Quantum Electron. **11**, 874 (1975).
9. S. T. Fard, W. Hofmann, P. T. Fard, G. Bohm, M. Ortsiefer, E. Kwok, M. C. Amann, and L. Chrostowski, IEEE Photon. Technol. Lett. **20**, 930 (2008)
10. F.J. McAleavey, J. O'Gorman, J.F. Donegan, B.D. MacCraith, J. Hegarty, G. Mazé, IEEE J. Sel. Top. Quant. Electron. **3** ,1103 (1997).
11. M. E. Webber, J. Wang, S. T. Sanders, D. S. Baer, and R. K. Hanson, Proc. Combust. Inst. **28**, 407 (2000).
12. P. Loiko, R. Soulard, L. Guillemot, G. Brasse, J.-L. Doulan, A. Braud, A. Tyazhev, A. Hideur, B. Guichardaz, F. Druon, and P. Camy, IEEE J. Quantum Electron. **55**, 1700212 (2019).
13. L. Guillemot, P. Loiko, E. Kifle, J.-L. Doualan, A. Braud, F. Starecki, T. Georges, J. Rouvillain, A. Hideur, and P. Camy, Opt. Mater. **101**, 109745 (2020).
14. L. Guillemot, P. Loiko, R. Soulard, A. Braud, J.-L. Doualan, A. Hideur, and P. Camy, Opt. Express **28**, 3451 (2020).
15. P. Loiko, E. Kifle, L. Guillemot, J.-L. Doualan, F. Starecki, A. Braud, M. Aguiló, F. Díaz, X. Mateos, and P. Camy, J. Opt. Soc. Am. B 38(2), 482-495 (2021).
16. E. Kifle, P. Loiko, L. Guillemot, J.-L. Doualan, F. Starecki, A. Braud, T. Georges, J. Rouvillain, and P. Camy, Appl. Opt. **59**, 7530 (2020).
17. S. Wang, H. Yu, H. Zhang, A. Wang, M. Zhao, Y. Chen, L. Mei, and J. Wang, Adv. Mater. 26(21), 3538–3544 (2014).
18. J. M. Serres, P. Loiko, X. Mateos, H. Yu, H. Zhang, Y. Chen, V. Petrov, U. Griebner, K. Yumashev, M. Aguiló, and F. Díaz, Opt. Mater. Express 6(10), 3262-3273 (2016).
19. F. Y. Zha, H. W. Chu, Z. B. Pan, H. Pan, S. Z. Zhao, M. Yang and D. C. Li, Opt. Lett. **47**, 3271 (2022).
20. J.M. Serres, P. Loiko, X. Mateos, K. Yumashev, U. Griebner, V. Petrov, M. Aguiló, and F. Díaz, Opt. Express 23(11), 14108–14113 (2015).
21. A.S. Yasukevich, P. Loiko, N.V. Gusakova, J.M. Serres, X. Mateos, K.V. Yumashev, N.V. Kuleshov, V. Petrov, U. Griebner, M. Aguiló, and F. Díaz, Opt. Commun. 389, 15-22 (2017).
22. E. Kifle, P. Loiko, L. Guillemot, J.-L. Doualan, F. Starecki, A. Braud, A. Hideur, and P. Camy, Opt. Commun. **500**, 127219 (2021).
23. F. Y. Wu, S. Q. Wang, H. W. Chen, and H. T. Huang, Front. Inform. Tech. Electron. Eng. **22**, 312 (2021).
24. S. Q. Wang, H. T. Huang, H. W. Chen, X. Liu, S. D. Liu, J. L. Xu, and D. Y. Shen, Continuum **2**, 1676 (2019).
25. F. Canbaz, I. Yorulmaz, and A. Sennaroglu, Opt. Lett. **42**, 1656 (2017).
26. L. Dong, H. W. Chu, Z. B. Pan, Y. Li, S. Z. Zhao, and D. C. Li, Opt. Mater. **131**, 112724 (2022).
27. H. W. Chu, L. Dong, Z. Pan, X. Ma, S. Zhao, and D. C. Li, Opt. Laser Technol. **147**, 107679 (2022).

1. E. C. Honea, R. J. Beach, S. B. Sutton, J. A. Speth, S. C. Mitchell, J. A. Skidmore, M. A. Emanuel, and S. A. Payne, "115W Tm:YAG diode-pumped solid-state laser," IEEE J. Quantum Electron. **33**, 1592 (1997).
2. J. B. Gruber, M. E. Hills, R. M. Macfarlane, C. A. Morrison, G. A. Turner, G. J. Quarles, G. J. Kintz and L. Esterowitz, "Spectra and energy levels of Tm^{3+}: $Y_3Al_5O_{12}$," Phys. Rev. B. **40**, 9464 (1989).
3. R.C. Stoneman, and L. Esterowitz, "Efficient, broadly tunable, laser-pumped Tm: YAG and Tm: YSGG cw lasers," Opt. Lett. **15**, 486 (1990).
4. L.J. Li, L. Zhou, T.X. Li, X.N. Yang, W.Q. Xie, X.M. Duan, Y.J. Shen, Y.Q. Yang , W.L. Yang, H. Zhang, "Passive mode-locking operation of a diode-pumped Tm: YAG laser with a MoS_2 saturable absorber," Opt. Laser Technol. **124**, 105986 (2020).
5. J. I. Mackenzie, S.C. Mitchell, R.J. Beach, H.E. Meissner, D.P. Shepherd, "15 W diode-side-pumped Tm: YAG waveguide laser at 2μm," Electron. Lett. **37**, 898 (2001).
6. J. Zhang, F. Schulze, K.F. Mak, V. Pervak, D. Bauer, D. Sutter, O. Pronin, "High - power, high - efficiency Tm: YAG and Ho: YAG thin-disk lasers," Laser Photon. Rev. **12**, 1700273-1-6 (2018).
7. A. Braud, S. Girard, J.L. Doualan, M. Thuau, R. Moncorge, A.M. Tkachuk, "Energy-transfer processes in Yb, Tm: -doped KY_3F_{10}, $LiYF_4$, and BaY_2F_8 single crystals for laser operation at 1.5 and 2.3 μm," Phys. Rev. B. **61**, 5280 (2000).
8. J. Caird, L. DeShazer, and J. Nella, "Characteristics of room-temperature 2.3μm laser emission from Tm^{3+} in YAG and $YAlO_3$," IEEE J. Quantum Electron. **11**, 874 (1975).
9. S. T. Fard, W. Hofmann, P. T. Fard, G. Bohm, M. Ortsiefer, E. Kwok, M. C. Amann, and L. Chrostowski, "Optical absorption glucose measurements using 2.3μm vertical-cavity semiconductor lasers," IEEE Photon. Technol. Lett. **20**, 930 (2008)
10. F.J. McAleavey, J. O'Gorman, J.F. Donegan, B.D. MacCraith, J. Hegarty, G. Mazé, "Narrow linewidth, tunable Tm^{3+}-doped fluoride fiber laser for optical-based hydrocarbon gas sensing," IEEE J. Sel. Top. Quant. Electron. **3** ,1103 (1997).
11. M. E. Webber, J. Wang, S. T. Sanders, D. S. Baer, and R. K. Hanson, "In situ combustion measurements of CO, CO_2, H_2O and temperature using diode laser absorption sensors," Proc. Combust. Inst. **28**, 407 (2000).
12. P. Loiko, R. Soulard, L. Guillemot, G. Brasse, J.-L. Doulan, A. Braud, A. Tyazhev, A. Hideur, B. Guichardaz, F. Druon, and P. Camy, "Efficient Tm: $LiYF_4$ lasers at ∼2.3 μm: effect of energy-transfer upconversion," IEEE J. Quantum Electron. **55**, 1700212 (2019).
13. L. Guillemot, P. Loiko, E. Kifle, J.-L. Doualan, A. Braud, F. Starecki, T. Georges, J. Rouvillain, A. Hideur, and P. Camy, "Watt-level mid-infrared continuous-wave Tm: YAG laser operating on the $^3H_4 \rightarrow {}^3H_5$ transition," Opt. Mater. **101**, 109745 (2020).
14. L. Guillemot, P. Loiko, R. Soulard, A. Braud, J.-L. Doualan, A. Hideur, and P. Camy, "Close look on cubic Tm:KY_3F_{10} crystal for highly efficient lasing on the $^3H_4 \rightarrow {}^3H_5$ transition," Opt. Express **28**, 3451 (2020).
15. P. Loiko, E. Kifle, L. Guillemot, J.-L. Doualan, F. Starecki, A. Braud, M. Aguiló, F. Díaz, X. Mateos, and P. Camy, "Highly-efficient ~2.3 μm Thulium lasers based on a high-phonon-energy crystal: evidence of vibronic-assisted emissions," J. Opt. Soc. Am. B 38(2), 482-495 (2021).
16. E. Kifle, P. Loiko, L. Guillemot, J.-L. Doualan, F. Starecki, A. Braud, T. Georges, J. Rouvillain, and P. Camy, "Watt-level diode-pumped thulium lasers around 2.3 μm," Appl. Opt. **59**, 7530 (2020).
17. S. Wang, H. Yu, H. Zhang, A. Wang, M. Zhao, Y. Chen, L. Mei, and J. Wang, "Broadband few-layer MoS2 saturable absorbers," Adv. Mater. 26(21), 3538–3544 (2014).
18. J. M. Serres, P. Loiko, X. Mateos, H. Yu, H. Zhang, Y. Chen, V. Petrov, U. Griebner, K. Yumashev, M. Aguiló, and F. Díaz, "MoS_2 saturable absorber for passive Q-switching of Yb and Tm microchip lasers," Opt. Mater. Express 6(10), 3262-3273 (2016).
19. F. Y. Zha, H. W. Chu, Z. B. Pan, H. Pan, S. Z. Zhao, M. Yang and D. C. Li, "Large-scale few-layered MoS_2 as a saturable absorber for Q-switching operation at 2.3 μm," Opt. Lett. **47**, 3271 (2022).
20. J.M. Serres, P. Loiko, X. Mateos, K. Yumashev, U. Griebner, V. Petrov, M. Aguiló, and F. Díaz, "Tm:KLu(WO4)2 microchip laser Q-switched by a graphene-based saturable absorber," Opt. Express 23(11), 14108–14113 (2015).
21. A.S. Yasukevich, P. Loiko, N.V. Gusakova, J.M. Serres, X. Mateos, K.V. Yumashev, N.V. Kuleshov, V. Petrov, U. Griebner, M. Aguiló, and F. Díaz, "Modeling of graphene Q-switched Tm lasers," Opt. Commun. 389, 15-22 (2017).
22. E. Kifle, P. Loiko, L. Guillemot, J.-L. Doualan, F. Starecki, A. Braud, A. Hideur, and P. Camy, "Design and modeling of a passively Q-switched diode-pumped Thulium laser at 2.3 μm," Opt. Commun. **500**, 127219 (2021).
23. F. Y. Wu, S. Q. Wang, H. W. Chen, and H. T. Huang, "2.3 μm nanosecond passive Q-switching of an LD-pumped Tm:YLF laser using gold nanorods as a saturable absorber," Front. Inform. Tech. Electron. Eng. **22**, 312 (2021).
24. S. Q. Wang, H. T. Huang, H. W. Chen, X. Liu, S. D. Liu, J. L. Xu, and D. Y. Shen, "High efficiency nanosecond passively Q-switched 2.3 μm Tm:YLF laser using a $ReSe_2$-based saturable output coupler," OSA Continuum **2**, 1676 (2019).
25. F. Canbaz, I. Yorulmaz, and A. Sennaroglu, "2.3-μm Tm^{3+}:YLF laser passively Q-switched with a Cr^{2+}:ZnSe saturable absorber," Opt. Lett. **42**, 1656 (2017).
26. L. Dong, H. W. Chu, Z. B. Pan, Y. Li, S. Z. Zhao, and D. C. Li, "Synthesis of core-shell polyhedron ZIF-8@ZIF-67 as saturable absorber for passive Q-switching operation in Tm:YAP laser at $^3H_4 \rightarrow {}^3H_5$ transition," Opt. Mater. **131**, 112724 (2022).
27. H. W. Chu, L. Dong, Z. Pan, X. Ma, S. Zhao, and D. C. Li, "Passively Q-switched Tm:YAP laser with a zeolitic imidalate framework-67 saturable absorber operating at $^3H_4 \rightarrow {}^3H_5$ transition," Opt. Laser Technol. **147**, 107679 (2022).